INSTITUTE OF PHYSICS PUBLISHING NETWORK: COMPUTATION IN NEURAL SYSTEMS

Network: Comput. Neural Syst. **14** (2003) 103–118 PII: S0954-898X(03)57829-0

Information encoding and computation with spikes and bursts

Adam Kepecs and John Lisman

Volen Center for Complex Systems, Brandeis University, 415 South Street, Waltham, MA 02454, USA

E-mail: kepecs@cshl.org

Received 8 April 2002, in final form 25 December 2002
Published 17 January 2003
Online at stacks.iop.org/Network/14/103

Abstract

Neurons compute and communicate by transforming synaptic input patterns into output spike trains. The nature of this transformation depends crucially on the properties of voltage-gated conductances in neuronal membranes. These intrinsic membrane conductances can enable neurons to generate different spike patterns including brief, high-frequency bursts that are commonly observed in a variety of brain regions. Here we examine how the membrane conductances that generate bursts affect neural computation and encoding. We simulated a bursting neuron model driven by random current input signal and superposed noise. We consider two issues: the timing reliability of different spike patterns and the computation performed by the neuron. Statistical analysis of the simulated spike trains shows that the timing of bursts is much more precise than the timing of single spikes. Furthermore, the number of spikes per burst is highly robust to noise. Next we considered the computation performed by the neuron: how different features of the input current are mapped into specific output spike patterns. Dimensional reduction and statistical classification techniques were used to determine the stimulus features triggering different firing patterns. Our main result is that spikes, and bursts of different durations, code for different stimulus features, which can be quantified without *a priori* assumptions about those features. These findings lead us to propose that the biophysical mechanisms of spike generation enables individual neurons to encode different stimulus features into distinct spike patterns.

1. Introduction

Neurons transform the continuous barrage of synaptic input into sequences of action potentials. The neural code is determined by the attributes of these output spike sequences that are relevant for other neurons. The input–output transformation constitutes the computation performed by

the neuron. In this paper we study how certain biophysical properties and active conductances of neurons determine the nature of the input–output transformation and place constraints on neural coding.

As a first approximation, neurons fire action potentials with a frequency proportional to the magnitude of the input current. This transformation depends on the properties of the fast sodium and potassium currents underlying spike generation [22]. Much of the complexity behind the spike generation process can be captured by 'leaky' integration of inputs followed by a thresholding process [26]. This leads to 'forgetful' integrate-and-fire models that can match the overall statistics of spike trains [8, 40, 52] and have been widely used to support neural coding arguments [46, 50]. According to these proposals, a single variable—the rate of spiking—contains the only useful information. This leads to an instantaneous spike code where correlations between spikes are assumed not to carry information [46, 49], hence at the single-neuron level coding issues are restricted to the relevant timescales and the reproducibility of spiking [1].

However, these kinds of simplified neuron models do not incorporate the numerous biophysical mechanisms that are known to exist in real neurons. For instance, the active membrane processes [5, 27, 37] of distributed dendritic structures [31, 33] have a significant impact on synaptic integration and spike generation. Recent studies have considered how active dendrites [20], stochastic ion channels [44] and noise in dendritic cable structures [32] constrain neural information processing. Here, we ask how the active membrane currents that generate bursts of action potentials affect neural coding and computation.

We focus on bursting because it is both widely studied as an intrinsic property of neurons *in vitro* [3, 30] and at the same time considerable evidence has been accumulating about the role of bursts in neural coding *in vivo* [28, 47]. Hippocampal neurons show tighter place-fields [35, 36], feature selectivity of some neurons in the visual cortex is sharpened [11, 29] and feature extraction by electric fish pyramidal cells is more reliable [18] when only spikes belonging to bursts are considered. In area MT of monkeys, the rate of burst events was found to reflect the direction of the visual stimulus better than the mean firing rate [4]. In the visual thalamus bursts have been found to encode stimuli at a higher efficiency that single spikes [41, 42]. Most of these studies concentrated on the idea that bursts are more *reliable* coding elements and did not address whether they carry information *distinct* from that of single spikes. This is important because it has been observed that certain spikes have differential stimulus selectivities depending on the preceding inter-spike-interval (ISI) [13, 39].

We approach these issues from a biophysical perspective, by trying to identify what neural codes the mechanisms of bursting might support. We use a model bursting neuron that incorporates the minimal ingredients for burst generation in hippocampal and cortical neurons and belongs to a large class of models with similar properties [24]. When driven by random current injections this model fires both single spikes and bursts of spikes, which allows us to make comparisons within the same spike train. Our previous results showed that bursts are triggered when the input current is increasing and the spike count of a burst encodes the rate of increase [25]. Here we test the encoding differences between bursts and spikes without specific assumptions about the features encoded. We consider two broad issues.

(i) Are bursts more reliable than single spikes simply as a consequence of their underlying biophysical mechanisms?

(ii) Are bursts triggered by different stimulus features than single spikes?

Our findings reveal that simple biophysical mechanisms can greatly enhance the reliability and coding complexity of neurons.

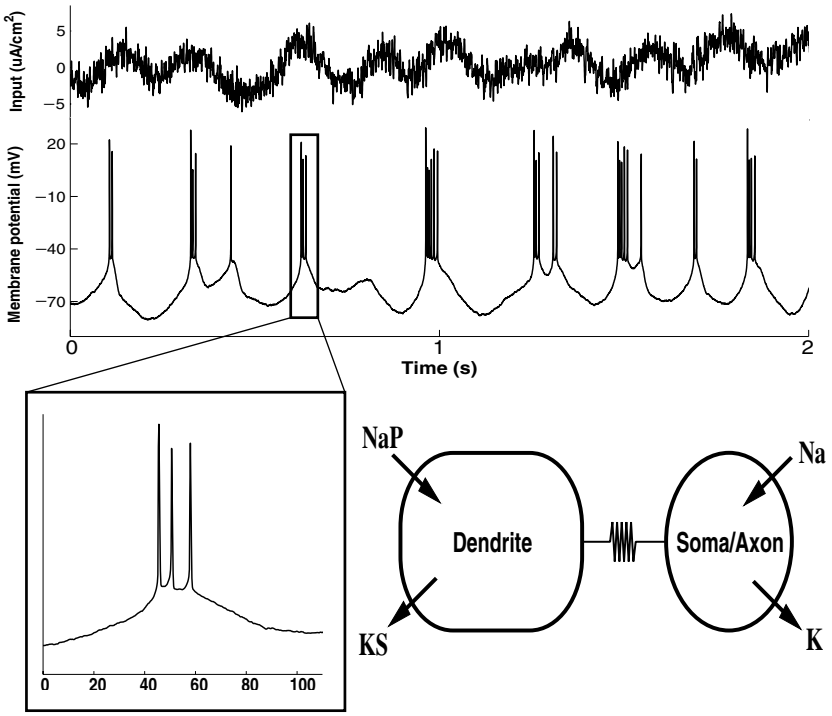

Figure 1. Biophysical model of burst firing. The upper trace shows an example of the input signal, random current with 5 Hz cut-off, with white noise added. The stimulus was smoothed for better visualization. The membrane voltage response is shown below. The spike train contains both single spikes and bursts. The right-hand panel shows the structure of the model.

2. Methods

2.1. Bursting neuron model

We use a model neuron that can fire isolated as well as bursts of spikes (figure 1). The model is comprised of two compartments: an axon/soma compartment with spiking currents and a dendritic compartment, which contains the currents responsible for bursting (figure 1). These ingredients reflect the minimal biophysical mechanisms necessary to reproduce burst firing in pyramidal cells [23, 24, 38, 51]. The neural membranes obey the following current-balance equations:

$$C_m \mathrm{d}V_s/\mathrm{d}t = -I_{\mathrm{Na}} - I_{\mathrm{K}} - I_{Leak} - g_c(V_s - V_d)/p + I_{soma} \tag{1}$$

$$C_m \mathrm{d}V_d/\mathrm{d}t = -I_{\mathrm{NaP}} - I_{\mathrm{KS}} - I_{Leak} - g_c(V_d - V_s)/(1-p) + I_{dendrite}. \tag{2}$$

The individual conductances were simulated using a Hodgkin–Huxley formalism as described in the appendix. This model belongs to the class of square-wave bursters [43] with the dendritic potassium current acting as the slow parameter [24]. The role of the fast inward current, I_{NaP}, in the dendrites is to produce a regenerative current that drives the high firing rate during a burst (100–300 Hz). The role of the slowly activating dendritic K^+ current is to terminate the regenerative inward current and thereby bring an end to the burst (figure 1, inset).

We stimulated the model neuron with random current injections. To generate the input signal we inverse Fourier transformed a flat power spectrum with a cut-off frequency, f_c,

resulting in correlations at a timescale $\tau_{corr} = 1/2f_c$. We have obtained similar results with low cut-off frequencies in the range of 2–20 Hz, and report here simulations with $f_c = 5$ Hz because bursting neurons behave like band-pass filters in terms of their preferred frequencies. This type of input can be considered to represent a summation of stochastic inputs modulated up to a characteristic frequency, f_c. To examine the effects of noise, we added Gaussian white noise to the signal, typically with a standard deviation twice that of the signal. Figure 1 shows an example trace of a stimulus segment with noise added. The resulting spike train is highly irregular, containing mostly bursts of different durations and occasional single spikes. We obtained qualitatively similar results with a range of input statistics. In the simulations reported here the random input current is normally distributed with a mean of 0.6 μA cm^{-2} and a standard deviation of 1.8 μA cm^{-2}. Simulations were run for 100 min of simulated time with a mean firing rate of 14 Hz. Simulations with white noise, N(0, 3.6) in μA cm^{-2}, added to the input signal were run for 2 min each for 60 trials.

2.1.1. Spike train segmentation. In order to examine the coding properties of bursts and spikes separately, we first need to segment the spike train. A standard technique to determine whether a spike belongs to a burst or not is to use the shape of the ISI histogram (e.g. [18]). Figure 2(A) shows that the ISI histogram is bimodal with a very pronounced peak for short ISIs followed by longer intervals that can be better appreciated on a log scale [39]. For instance, a spike can be classified as the first spike of a burst if the following ISI is below a certain threshold, Θ_B. The rest of the burst consists of spikes that are preceded by ISIs below this threshold value. Spikes belonging to bursts can then be visualized as an L-shaped region on the ISI return map (figure 2(B)). In cortical and hippocampal neurons the typical ISI threshold value, Θ_B, is 4–6 ms [21, 39], but for instance in electric fish significantly higher numbers (10–25 ms) have also been reported [34]. The conductance kinetics of our model are consistent with *in vitro* data [3] and are therefore slower. The corresponding cumulative ISI probability distributions (figure 2(C)) show distinct plateaus that can guide us in choosing an appropriate ISI threshold for burst segmentation. For the simulations presented here, the plateau value is reached at around 15 ms. Using this threshold value we segment the spike train into burst spikes and single spikes. The first spike of bursts is used to represent bursts as events (BE). Figure 2(C) shows separate histograms for these distinct spike groups. Slight changes in Θ_B did not affect our results. After determining which spikes belong to bursts we can further classify spike groups depending on the number of spikes per burst. Since the time duration is proportional to the number of spikes per burst we will also refer to the spike count in bursts as the burst duration.

For the noise analysis we have also used another segmentation method that allows the alignment of bursts and other firing events across trials [7]. We identified firing events by first smoothing the post-stimulus time histogram (PSTH) with a Gaussian filter with a standard deviation of 20 ms and then separated events at the intervening minima. The timing jitter of each event was calculated using the timing of the first spikes of events (when present) with the mean subtracted.

2.1.2. Spike-triggered covariance analysis. To identify the stimulus features encoded by the neuron we used the spike-triggered covariance method [2, 10, 13, 45]. We represent the time-varying stimulus, $s(t)$, as an N-dimensional vector preceding spikes by time period τ discretized at $\Delta t = \tau/N$ precision, $\boldsymbol{s}_t = s(t - \tau : \Delta t : t)$ with $\tau = 400$ ms and $\Delta t = 5$ ms. We calculate the spike-triggered covariance matrix for all spikes,

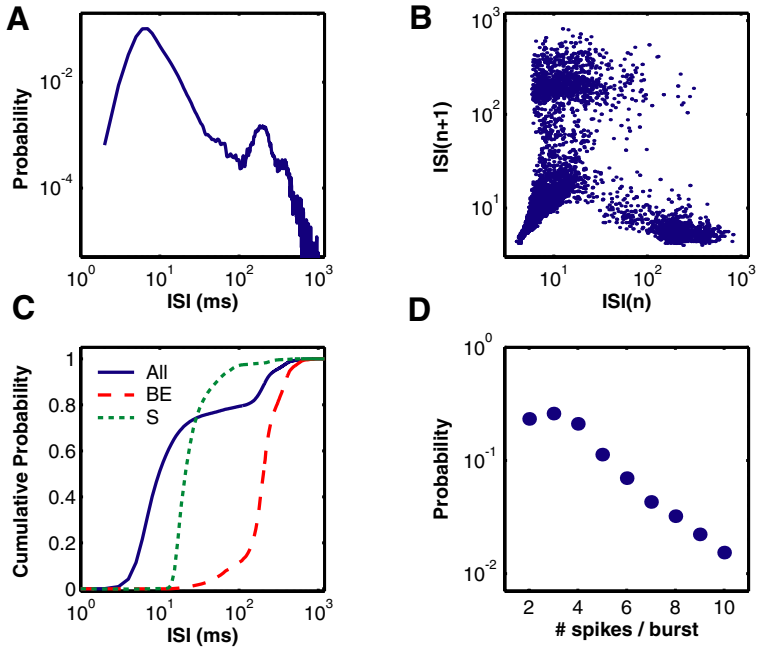

Figure 2. Inter-spike structure of bursts. (A) Inter-spike interval histogram shows two timescales on a logarithmic scale. (B) The inter-spike interval (ISI) return map represents each spike as a function of the preceding and following interspike intervals. (C) Cumulative event histograms for all spikes, for BE and for single spikes (S). (D) Probability distribution for bursts of different spike counts in logarithmic coordinates.

$$C_{\mathcal{A}} = \frac{1}{N_{\mathcal{A}} - 1} \sum_{t \in \mathcal{A}} (\boldsymbol{s}_t - \boldsymbol{\mu}_{\mathcal{A}})(\boldsymbol{s}_t - \boldsymbol{\mu}_{\mathcal{A}})^{\mathrm{T}} \tag{3}$$

where $\mathcal{A}$ represents the set of all spikes ($\tau \leqslant t \leqslant T$), $N_{\mathcal{A}}$ the number of spikes and $\boldsymbol{\mu}_A$ is the spike-triggered average,

$$\boldsymbol{\mu}_{\mathcal{A}} = \frac{1}{N_{\mathcal{A}}} \sum_{t \in \mathcal{A}} \boldsymbol{s}_t. \tag{4}$$

The relevant stimulus features can be identified with dimensionality reduction of the 'difference covariance' matrix, $\Delta C_{\mathcal{A}} = C_{\mathcal{A}} - C_{prior}$, where C_{prior} is the covariance matrix of the entire input signal. These matrices are N by N dimensional ($N = \tau/\Delta t$). Principal component analysis is used to find the eigenvectors associated with the eigenvalues of $\Delta C_{\mathcal{A}}$ that capture most of the variance. The subscript $\mathcal{A}$ signifies triggering on all spikes, while $\mathcal{B}$ and $\mathcal{S}$ refer to bursts and single spikes.

2.1.3. Multiple discriminant analysis. Multiple discriminant analysis (MDA) allows us compare the feature selectivity of multiple classes of spike patterns [14]. Given predefined classes of spikes, MDA finds the stimulus directions that discriminate between these classes the most. The basic idea is to separate the total scatter of data points, $\boldsymbol{S}_T$, into two parts, the sum of scatters within each class, $\boldsymbol{S}_W$, and the scatter between classes, $\boldsymbol{S}_B$. The within class scatter is defined as the sum of the individual covariance matrices for each class times $(N_i - 1)$,

where N_i is the number of events in class i,

$$\boldsymbol{S}_W = \sum_{i=1}^{c}(N_i - 1)\boldsymbol{C}_i = \sum_{i=1}^{c}(N_i - 1)\sum_{t\in\mathcal{C}_i}, (\boldsymbol{s}_t - \boldsymbol{\mu}_i)(\boldsymbol{s}_t - \boldsymbol{\mu}_i)^{\mathrm{T}} \tag{5}$$

$$\boldsymbol{S}_B = \sum_{i=1}^{c} N_i(\boldsymbol{\mu}_i - \boldsymbol{\mu})(\boldsymbol{\mu}_i - \boldsymbol{\mu})^{\mathrm{T}} \tag{6}$$

where $\boldsymbol{\mu}_i$ is the spike-triggered average for a given class of spikes and $\boldsymbol{\mu}$ is the spike-triggered average across all spikes. We are seeking a projection $\boldsymbol{s}' = \boldsymbol{D}^{\mathrm{T}}\boldsymbol{s}$ that best separates the classes. The classes are well separated if the within class scatter, $\boldsymbol{S}_W$, is minimal, while the between class scatter, $\boldsymbol{S}_B$, is large. This intuition can be quantified with the criterion function

$$J(\boldsymbol{D}) = \frac{\boldsymbol{D}^{\mathrm{T}}\boldsymbol{S}_B\boldsymbol{D}}{\boldsymbol{D}^{\mathrm{T}}\boldsymbol{S}_W\boldsymbol{D}}. \tag{7}$$

To find an optimal transformation matrix $\boldsymbol{D}$ that separates our classes, we need to maximize J. This can be achieved by transforming the problem into a generalized eigenvalue problem: $\boldsymbol{S}_B\boldsymbol{d}_i = \lambda_i\boldsymbol{S}_W\boldsymbol{d}_i$, where $\boldsymbol{d}_i$ are the columns of the optimal $\boldsymbol{D}$ matrix [14].

3. Results

We simulated a model bursting neuron with random current input (f_c = 5 Hz, mean = 0.6, std = 1.8 in μA cm^{-2}). In some simulations we added white noise (std = 3.6 μA cm^{-2}) on top of the random signal in successive trials. Under these conditions, the model neuron fires a mixture of single spikes and bursts (figure 1). The spike count of bursts follows a roughly exponential distribution with only two spike bursts diverging from this trend appreciably (figure 2(D)). The shape of this distribution is similar to what has been observed in pyramidal neurons of weakly electric fish [34] and hippocampal pyramidal cells [21].

3.1. Reliable timing and spike count in bursts

Figure 3 shows that despite a significant noise current, the model can fire sparse spike events that are well aligned across different trials. Visual inspection of different firing events already reveals that single spikes tend to occur less reliably than bursts (figure 4(A)). Notice that after the first spike of the burst is initiated, the rest of the spikes show a fairly stereotyped pattern. Due to the effects of noise it was not always possible to unambiguously relate single spikes and bursts occurring in different trials. Therefore to quantitatively examine the reproducibility of different firing patterns we segmented the responses into different firing events [7]. Visual examination showed that most of these firing events do correspond to burst events, although in some cases single spikes and bursts were classified together into a single event.

For each event we calculated the mean and the variance of the spike count. Figure 4(B) shows that most events are highly stereotyped and thus have very low count variances. However, for some events with low mean counts the variance was sometimes proportional to the mean, as expected for a Poisson process. The stereotyped nature of these events can be appreciated by looking at the probability histogram of events with different spike counts (figure 4(D)). Not only did events exhibit low variability in spike count, most events in fact diverged little from a stereotyped, integer count and had negligible variance.

We next considered the timing jitter of these firing events. Figure 4(C) shows the timing variability of events as a function of the mean count. Events with low mean count (<2) show considerable variability. Events containing two or more spikes are much less variable and variability decreases systematically with increasing mean spike count. Because most firing

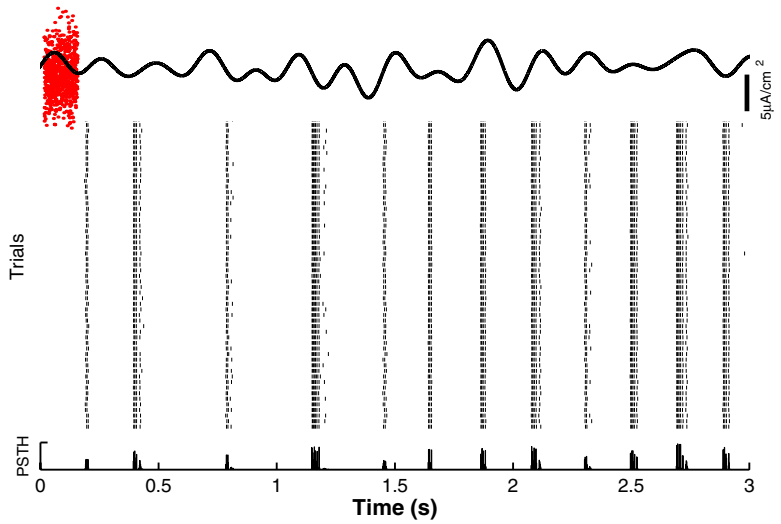

Figure 3. Reproducible timing of burst events. The input signal used was random current with 5 Hz cut-off frequency having a mean 0.6 and standard deviation 1.8 (μA cm^{-2}). In different trials, independent white noise was added with a standard deviation of 3.6 (μA cm^{-2}), a portion of which is plotted on the left. The PSTH has a scale bar of 120 Hz.

events correspond to bursts, these results can be understood by considering the biophysical mechanisms underlying bursts. Once a burst is triggered, the inward current underlying it produces a large regenerative current that drives the high firing rate during a burst. When this current dominates, external noise sources have little effect on the spike generating currents in the somatic compartment. The longer the burst, the larger the regenerative event underlying it and therefore the less sensitive it is to noise.

3.2. Mapping the computation performed by spikes and bursts

These measurements show that different spike patterns have distinct coding properties in terms of timing precision. However, this does not address another meaning of spike pattern encoding when different firing patterns carry different kinds of information. For instance, bursts and spikes could carry the same *amount* of stimulus-related information about different *features* of the stimulus. We analyse this issue by finding a low-dimensional representation of the stimulus triggering spikes and bursts. The mapping from this feature space to specific spike patterns constitutes the computation performed by the neuron.

3.2.1. Geometry of spike patterns in feature space. To find the relevant stimulus features for our neuron, we use the spike-triggered covariance method [2, 13]. The goal of the method is to identify the relevant stimulus subspace where most of the response-specific attributes of stimuli are concentrated. This requires calculating the change in stimulus covariance ΔC_{spike} preceding spike initiation. The change in covariance matrix is $\Delta C_{spike} = C_{spike} - C_{prior}$, where C_{spike} is the spike-triggered covariance matrix and C_{prior} is the covariance matrix of the entire input signal. We discretize the signal at 5 ms and look back at the 400 ms period preceding spikes. This results in (80 by 80)-dimensional covariance matrices. Figure 5(A) shows the spike-triggered covariance matrix calculated for all spikes. Because we were interested in

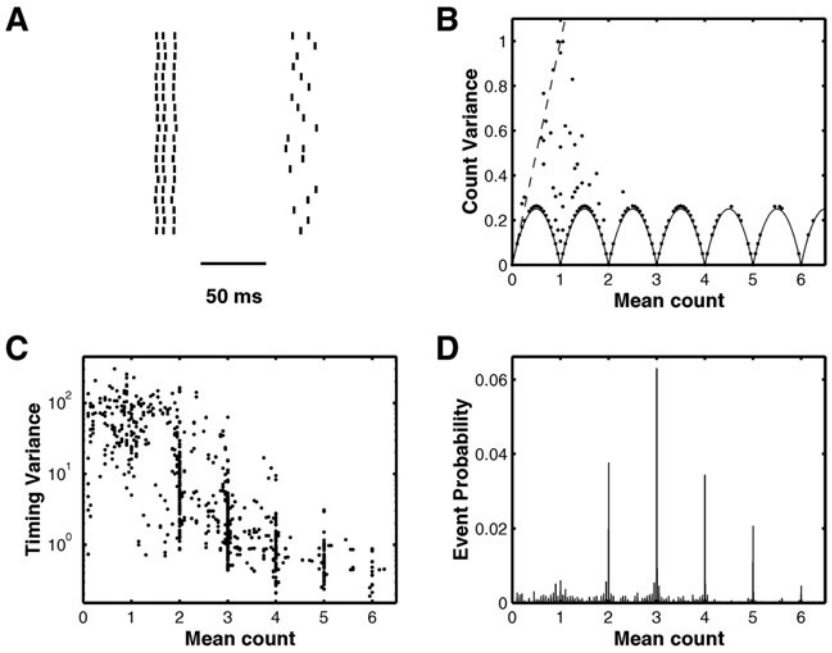

Figure 4. Spike train statistics. (A) Example traces showing a segment of the spike train across 20 trials. Notice that the timing of the burst is more variable than its detailed structure. (B) The variance of spike count versus the mean spike count per burst event. Each point represents the variance of an event calculated from 60 trials. The dashed line shows the variance expected for a Poisson process, while the arches represent the minimum possible variance given that individual events have integer numbers of spikes. (C) The temporal jitter (variance) of the first spike of an event as a function of the mean spike count. Events under two spikes have the largest timing variance. The precision of timing increases dramatically with the number of spikes per event. (D) Histogram of event probability shows that most events have a stereotyped number of spikes.

comparing bursts and spikes we also calculated the 'single-spike-triggered', C_S, and the 'burst-spike-triggered', C_B, covariances. We determined the principal components of ΔC_B and ΔC_S to identify a lower-dimensional stimulus representation accounting for most of the variance in the data [17].

Figures 5(B) and (C) show the surprising finding that the eigenvectors corresponding the two largest eigenvalues of ΔC_B and ΔC_S are nearly identical. These two directions account for 90% of the variance of the stimulus preceding burst spikes in a 400 ms period, and 85% of the stimulus variance for single spikes. This means that both single spikes and bursts are selective to the same small subspace of the stimulus spanned by $\boldsymbol{e_1}$ and $\boldsymbol{e_2}$. Why should the subspace be common? This is probably due to the fact that the biophysical repertoire of the model determines the possible space of stimuli the neuron is selective to. The small dimensionality of this subspace is not entirely surprising, because by using a low cut-off frequency for the input signal we have already reduced the dimensionality of the stimulus distribution, i.e. C_{prior} is not of full rank. Notice that the eigenvector corresponding to the second largest eigenvalue, $\boldsymbol{e_2}$ (figure 5(C)), is approximately the derivative of the first mode, $\boldsymbol{e_1}$ (figure 5(B)), as already observed in both the H1 neuron of the blowfly [9], and a Hodgkin–Huxley model [2]. The corresponding eigenvalues (figures 5(D) and (E)) are different for spikes, $\boldsymbol{e}_i^S$, and bursts, $\boldsymbol{e}_i^B$, which already suggests that the feature selectivity of the average spike is different from that of the average burst. What is the meaning of these eigenvectors? They can be qualitatively

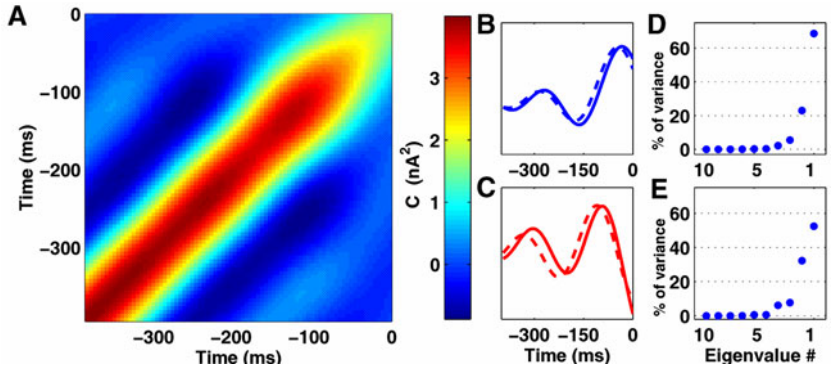

Figure 5. Spike-and burst-triggered covariance matrices have similar major eigenmodes. (A) The spike-triggered covariance matrix (C_{spike}) calculated over all spikes. (B) The eigenvectors corresponding to the largest eigenvalue for burst-spike-triggered ΔC_B (solid), and for the single-spike-triggered ΔC_S (dashed). (C) The eigenvectors corresponding to the second largest eigenvalue for burst-spike-triggered ΔC_B (solid) and for the single-spike-triggered ΔC_S (dashed). (D) The amount of the total variance explained by the eigenvalues of the burst-spike-triggered change in the covariance matrix. About 90% is explained by the two largest eigenvalues. Note that the prior covariance matrix was only of rank seven (eigenvalues $> 0.1\%$ total variance) due to the correlations induced by using a low cut-off frequency. (E) The total variance explained by the eigenvalues of the single-spike-triggered ΔC_S. About 85% is explained by the two largest modes. Notice that while the corresponding eigenvectors are similar, they account for a different portion of the variance compared with the case of bursts.

equated with the elementary features to which the neuron is selective. Both eigenvectors have differentiating components, which suggest that both bursts and spikes will be sensitive to the acceleration of current inputs and thus the neuron will not be purely integrating.

To examine how these stimulus filters, $\boldsymbol{e_1}$ and $\boldsymbol{e_2}$, correspond to specific firing patterns we project all the stimulus segments causing spikes, $\boldsymbol{s}_S$, and bursts, $\boldsymbol{s}_B$, onto the $(f_1, f_2) := (\boldsymbol{e_1}^{\mathrm{T}}\boldsymbol{s}_t, \boldsymbol{e_2}^{\mathrm{T}}\boldsymbol{s}_t)$ plane. Figure 6(A) shows the distribution of spikes and figure 6(B) the distribution of bursts in this space. Our major result is that bursts and spikes map onto different regions of the reduced stimulus space, demonstrating that they are selective to different stimulus features. Notice that both burst and spike distributions are narrower along $\boldsymbol{e_1}$ than $\boldsymbol{e_2}$ (figures 6(A) and (B)). Bursts are more selective along direction $\boldsymbol{e_1}$ (std $= 0.16$) than single spikes (std $= 0.22$). However, further considering other spike patterns, such as bursts of different spike counts, complicates this picture. Figure 6(C) shows the regions containing 90% of the single spikes (S), and burst events of different durations (2–5 spikes/burst). While there is significant overlap in these regions, the centres and shapes of the distributions are clearly different. These findings suggest that the computation performed by the neuron can be conceptualized as a two-step process. First the neuron filters stimuli onto a small feature space, $s(t) \mapsto (f_1, f_2)$, and then fires a specific firing pattern depending on the particular location in feature space $\mathcal{R}$: fire a given spike pattern when $(f_1, f_2) \in \mathcal{R}_{spike\ pattern}$.

3.2.2. Differential feature selectivity of spikes and bursts. Principal component analysis of spike-triggered covariance matrices is not designed to pick out differences between classes of spike patterns. The reason it works well in this model is because the subspace of spikes and bursts is nearly identical, which may not always hold (see discussion). Principal component analysis of ΔC finds the projections that best represent the data in the least-squares sense. If spike patterns encode different stimuli it might be that the differences between them lie outside

the common subspace. By restricting our analysis to the most *representative* directions we might be overlooking the most *discriminative* directions in stimulus space [17]. MDA is a useful tool that helps us find the most discriminating projection for multiple classes of spike patterns [14].

We calculated the discriminants, $\boldsymbol{d}_i$, for the feature separation between single spikes and bursts of different durations. Figure 7(A) shows the projection of different spike groups onto the two most significant discriminating directions. The first one, $\boldsymbol{d}_1$, accounts for about 75% of the scatter between spikes and burst events, while the second direction, $\boldsymbol{d}_2$ accounts for over 20%. While most spike groups are well separated there are a few 'stray' bursts in regions of single-spike triggering stimuli. This probably means that the single-ISI-based classification scheme could have missed further difference between different spike patterns.

Figure 7(B) shows the separation of single spikes and all burst events (not only two to five spike events) using a single discriminant, $\boldsymbol{d}_{\mathrm{SB}}$. Isolated spikes and bursts are well separated but a closer examination of the burst distribution shows that there is a 'bump' on the left-hand side (figure 7(B), arrow). This is a signature that the original class, burst events, is not homogeneous. In fact we found that the bump is caused by two spike bursts and disappears if the burst classification threshold, Θ_B, is made tighter (e.g. 10 ms). Unfortunately, then some spikes will be misclassified and a bump appears in the single-spike distribution. This again suggests that certain spike patterns are not separable by only considering a single ISI threshold. Using multiple ISIs for burst/spike classification or explicitly clustering spike patterns based on feature selectivity could further refine this spike pattern coding scheme. When we only considered how bursts of different durations differed, we found that a single discriminant, $\boldsymbol{d}_B$, could well separate four classes of bursts (figure 3(C)), suggesting that bursts of different durations convey information about the same stimulus feature.

The differences in the coding properties of different spike groups can be quantified by calculating the receiver operating characteristics (ROCs). This measure shows how well an ideal observer could distinguish between the occurrence of different spike groups based on an observation of the preceding stimulus segment. Figure 7(D) shows three examples calculated from the distributions in figures 7(B) and (C). Nearly perfect classification is possible for very low false alarm rates and the overall discriminability (area under the ROC curve) is above 95% for all these spike groups. Because a single (although different) discriminant can account for most of the differences between single spikes and bursts of different durations, one interpretation is that the computation performed by the neuron can be viewed as linear filtering followed by a threshold operation.

4. Discussion

It has been widely hypothesized that brief, high-frequency bursts of action potentials represent a special neural code. Here we have examined this issue using a biophysical model of bursting neurons stimulated with random current injections.

4.1. Bursts are robust symbols in the coding alphabet

Bursts can carry information about stimulus features in their *timing* and their *duration*. We find that the timing of bursts is much more reproducible across trials than the timing of isolated spikes, and the longer the burst, the more reliable it is (figure 4(C)). Burst patterns are highly stereotyped and their spike count is extremely robust to noise (figures 4(A) and (B)). Direct information calculations using the same model and parameters also show that the total information carried by bursts can be roughly accounted for by the timing of the first burst

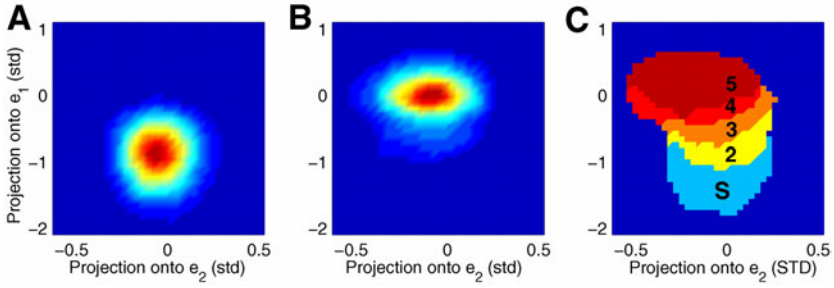

Figure 6. Geometry of burst and spike features. (A) Distribution of single spike causing stimuli projected onto the two eigenvectors of the two largest eigenvalues of the change in covariance matrix. (B) Distribution of burst causing stimuli. Notice that bursts are both more selective along direction e_1 and more different from single spikes. (C) Stimulus selectivity of spikes and bursts of different durations in the common stimulus subspace. Coloured regions contain 90% of events for a given spike pattern.

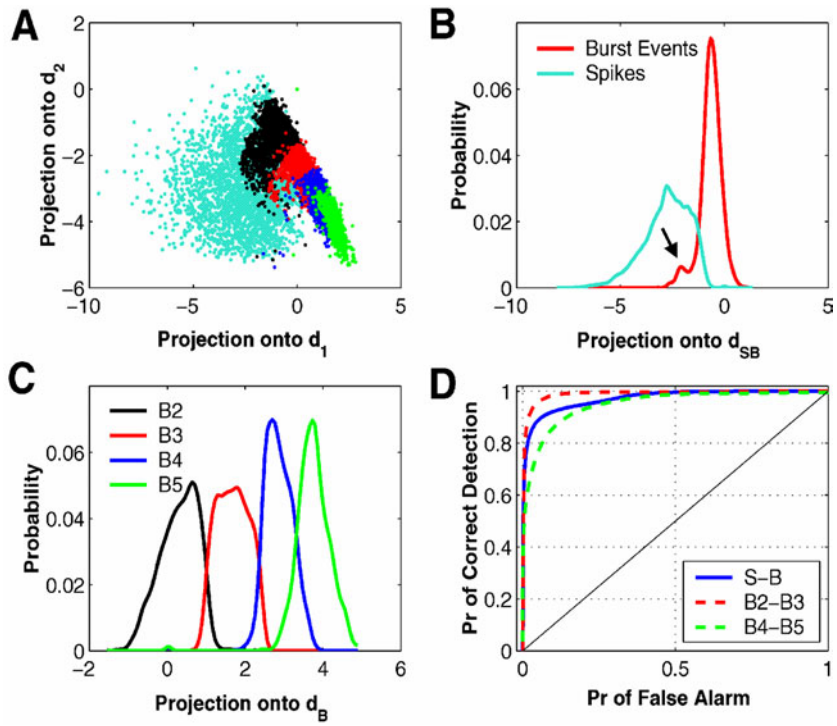

Figure 7. Spikes and bursts encode different stimulus features. (A) Stimulus segments causing spikes (cyan) and bursts of different durations (black 2, red 3, blue 4, green 5 spikes/burst) projected onto the discriminant plane (d_1 , d_2). Most spike patterns cluster well, and bursts of different duration seem to lie along a cone. (B) One-dimensional projection onto d_{SB}, the Fisher discriminant separating single spikes and burst events (first spikes of bursts of all durations). The bump on the left side of the burst distribution (arrow) is caused by two spike bursts with long inter-spike intervals. (C) One-dimensional projection onto d_B, the Fisher discriminant separating single bursts of different durations. Note that a single dimension separates well four classes of bursts. (D) ROC for an ideal observer trying to decide whether a given stimulus will result in a particular spike sequence. The probability of correct detection is plotted against the probability of false alarm. The diagonal represents chance level discrimination. S–B is a decision between single spikes and burst events in (B), B2–B3 (B4–B5) represents a decision between two and three (four and five) spike bursts shown in (C).

spike (70% of total) and the spike count (22% of total) (Kepecs, Garibay, Wang and Lisman, unpublished observations). While similar results are expected for high-rate spikes in a simple thresholding device combined with refractoriness [6], the large difference between single spikes and bursts shows that intrinsic factors are also significant. Once a burst is triggered, the contribution of intrinsic inward and outward currents dominates external noise sources leading to high precision.

It is tempting to speculate about how these results might relate to experimental evidence showing that bursts are more reliable codes than isolated spikes [18, 29]. For instance, many pyramidal neurons in weakly electric fish [53] and in neocortex [48] have intrinsic burst generation mechanisms, and these are likely to contribute to the observed reliability of bursts. Berry and Meister observed a similar event duration code in retinal ganglion cells, where the timing variability of firing events increased with the number of spikes per firing event [6]. They suggested that refractoriness could contribute to firing precision. In the context of intrinsic bursts it should be noted that the inward currents underlying bursts result in nearly maximal firing rates, thereby further exaggerating the role of refractoriness.

4.2. Feature extraction by spike patterns: a single-neuron computation

We also examined the features of the signal that bursts and spikes carry. Using spike-triggered covariance analysis we found that most of the variance is accounted for by two principal directions (figures 5(C), (D)) as previously shown both experimentally [9, 13] and in a Hodgkin–Huxley model [2]. Surprisingly, we found that both bursts and single spikes are selective largely to the same small stimulus subspace (figures 5(B), (C)). However, bursts and single spikes signal largely distinct regions of this subspace (figure 6). The differences between spike patterns were directly examined with discriminant analysis without restricting our attention to the common subspace. After projection onto the Fisher discriminant, stimuli triggering single spikes versus bursts could be distinguished with high accuracy (figures 7(B), (D)). Furthermore, a single discriminant could distinguish between stimuli triggering bursts of different durations (figure 7(C)). Thus bursts of different durations signal the degree to which a particular feature is present. These findings can account for our previous observations that bursts are triggered on the positive slopes of current input (note that the shapes of the filters in figures 5(B) and (C) can be interpreted as 'slope detecting') and burst duration signals the magnitude of the slope in a graded manner [25]. Importantly, the methods used here do not make any assumptions about the shapes of particular features or whether there is a difference in the feature selectivity of different spike patterns.

Our results suggest a conceptual picture of how single neurons compute in a two-stage fashion. In the first stage, they extract specific features of the stimulus using a set of filters. Then neurons fire the spike pattern associated with the particular combination of features. The set of filters is determined by the biophysical make-up of the neural membrane. Thus additional currents may make neurons selective to additional stimulus features and underlie the generation of more complex firing patterns to signal those features. Note that in general the stimulus selectivity of spike patterns need not be restricted to the same subspace and our findings (figures 5(B) and (C)) could be due to the simplicity of the neuron model used.

In the present work we only considered the temporal features of signals and did not examine the effects of morphology. In several brain regions, bursts can be regulated by distinct feedback pathways that provide input at different dendritic locations [5, 12, 27, 47]. For instance, if the location of input along a dendrite is varied it can (in-)activate selected sets of ion channels and thus change the filtering characteristics of the neuron. Furthermore, the (in-)activation of different ion channels can cause different spike patterns to be triggered.

Therefore different temporal and spatial patterns of input can, in principle, be encoded by distinct firing patterns. This picture of single-neuron computation is very different from previous suggestions about the roles of active currents. For instance, it has been suggested [33] that neurons compute locally non-linear functions combining them in a linear way and finally signalling the result in the output spike rate or count. Here we propose that specific spike patterns, such as bursts, can be used to multiplex information about different stimulus features.

We acknowledge that our modelling approach is laden with a number of assumptions about (i) the mechanisms of bursting, (ii) the detailed kinetics of ionic currents and (iii) the typical input patterns received by these neurons. While we could argue that (i) our model represents a large class of bursting neurons, where (ii) the details of the conductances affect the qualitative results little and (iii) our input varies at the timescales of interest for many physiological processes, we prefer to view our work as an 'existence proof'. Using a not-so-unrealistic bursting neuron model, our results point to possible biophysical mechanisms and constraints in neural coding. These ideas can be tested experimentally either *in vitro* by stimulating individual neurons with complex current inputs, or at the functional level *in vivo* by mapping the stimulus selectivity of different spike patterns. Previous work has already shown that short spike sequences carry specific stimulus features in the blowfly [13], although the mechanisms of this are not known.

4.3. Spike pattern coding

It is important to relate these results to previous ideas about spike pattern coding. According to one interpretation of spike pattern coding, the same features are being encoded but the existence of correlation enhances information transfer. This could either be due to the larger variability of the spike pattern (rare events) or their greater resistance to noise. In this case we say that the spike group considered as an event shows synergy. On the other hand it is equally possible that different groups of spikes will encode *different* information. Thus, in principle it is possible that the total amount of information carried will not change, only the type of information encoded. In the H1 neuron of the fly it seems that both possibilities occur: different ISIs have different spike-triggered averages [13] and they also show an overall change in the absolute information carried, i.e. synergy [10]. Similar correlation codes at the network level have been suggested to use distributed spike sequences, syn-fire chains [16, 54] or synchronous firing events [15, 19] to represent distinct stimuli. On the other hand, there is also some evidence that different inter-spike intervals [39] or even short spike sequences can represent different stimulus features [13] at the level of individual neurons.

Here we have shown that the biophysics of single neurons can support a similar feature-specific correlation code. Because neurons contain a much wider complement of ionic currents than what we have used, it is likely that more complex spike pattern codes also exist. These ideas about spike pattern coding can be experimentally tested using multiple discriminant analysis without the need to make assumptions about what features of the input are being encoded.

Appendix

The voltage-dependent conductances are described using standard Hodgkin–Huxley formalism. The kinetics of a gating variable x are described by $\mathrm{d}x/\mathrm{d}t = \phi_x(\alpha_x(1-x)-\beta_x x) = \phi_x(x_\infty - x)/\tau_x$.

$I_{\mathrm{Na}} = g_{\mathrm{Na}} m_\infty^3 h(V - E_{\mathrm{Na}}), \qquad m_\infty = \alpha_m/(\alpha_m + \beta_m)$

$\alpha_m = -0.1(V + 31)/(\exp(-0.1(V + 31)) - 1), \qquad \beta_m = 4\exp(-(V + 56)/18)$

$\alpha_h = 0.07\exp(-(V + 47)/20), \qquad \beta_h = 1/(\exp(-0.1(V + 17)) + 1)$

$I_{\mathrm{K}} = g_{\mathrm{K}} n^4 (V - E_{\mathrm{K}})$

$\alpha_n = -0.01(V + 34)/(\exp(-0.1(V + 34)) - 1) \qquad \beta_n = 0.125\exp(-(V + 44)/80)$

$I_{\mathrm{NaP}} = g_{\mathrm{NaP}} r_\infty^3 (V - E_{\mathrm{Na}})$

$r_\infty = 1/(1 + \exp(-(V + 57.7)/7.7))$

$I_{\mathrm{KS}} = g_{\mathrm{KS}} q (V - E_{\mathrm{K}})$

$q_\infty = 1/(1 + \exp(-(V + 35)/6.5))$

$\tau_q = 200/(\exp(-(V + 55)/30) + \exp((V + 55)/30))$

$I_{Leak} = g_{Leak}(V - E_{Leak})$

$C_m = 1\ \mu\mathrm{F\,cm^{-2}}$, $p = 0.15$, $\phi_h = \phi_n = 3.33$, $g_c = 1$, $g_{Leak} = 0.18$, $g_{\mathrm{Na}} = 45$, $g_{\mathrm{K}} = 20$, $g_{\mathrm{NaP}} = 0.09$, $g_{\mathrm{KS}} = 0.9$ in $\mathrm{mS\,cm^{-2}}$. $E_{Leak} = -65$, $E_{\mathrm{Na}} = +55$, $E_{\mathrm{K}} = -90$ in mV. Numerical integration was performed with a fourth-order Runge–Kutta method using a 0.01 ms time step.

References

[1] Abbott L F and Sejnowski T J 1999 *Neural Coding and Distributed Representations* (Cambridge, MA: MIT Press)

[2] Agüera y Arcas B, Fairhall A L and Bialek W 2001 What can a single neuron compute? *Advances in Neural Information Processing Systems* vol 13, ed T K Leen, T G Dietterich and V Tresp (Cambridge, MA: MIT Press) pp 75–81

[3] Azouz R, Jensen M S and Yaari Y 1996 Ionic basis of spike after-depolarization and burst generation in adult rat hippocampal CA1 pyramidal cells *J. Physiol.* **492** 211–23

[4] Bair W, Koch C, Newsome W and Britten K 1994 Power spectrum analysis of bursting cells in area MT in the behaving monkey *J. Neurosci.* **14** 2870–92

[5] Bastian J and Nguyenkim J 2001 Dendritic modulation of burst-like firing in sensory neurons *J. Neurophys.* **85** 10–22

[6] Berry M J and Meister M 1998 Refractoriness and neural precision *J. Neurosci.* **18** 2200–11

[7] Berry M J, Warland D K and Meister M 1997 The structure and precision of retinal spike trains *Proc. Natl Acad. Sci. USA* **94** 5411–16

[8] Binder M D, Poliakov A V and Powers R K 1999 Functional identification of the input–output transforms of mammalian motoneurones *J. Physiol.* **93** 29–42

[9] Brenner N, Bialek W and de Ruyter van Steveninck R R 2000 Adaptive rescaling maximizes information transmission *Neuron* **26** 695–702

[10] Brenner N, Strong P, Koberle R, Bialek W and de Ruyter van Steveninck R R 2000 Synergy in the neural code *Neural Comput.* **12** 1531

[11] Cattaneo A, Maffei L and Morrone C 1981 Two firing patterns in the discharge of complex cells encoding different attributes of the visual stimulus *Exp. Brain Res.* **43** 115–18

[12] Cauller L J, Clancy B and Connors B W 1998 Backward cortical projections to primary somatosensory cortex in rats extend long horizontal axons in layer I *J. Comput. Neurol.* **390** 297–310

[13] de Ruyter van Steveninck R and Bialek W 1988 Real-time performance of a movement-sensitive neuron in the blowfly visual system: coding and information transfer in short spike sequences *Proc. R. Soc.* B **234** 379–414

[14] Duda R O, Hart P E and Stork D G 2001 *Pattern Classification* (New York: Wiley)

[15] Fries P, Neuenschwander S, Engel A K, Goebel R and Singer W 2001 Rapid feature selective neuronal synchronization through correlated latency shifting *Nature Neurosci.* **4** 194–200

[16] Frostig R D, Gottlieb Y, Vaadia E and Abeles M 1983 The effects of stimuli on the activity and functional connectivity of local neuronal groups in the cat auditory cortex *Brain Res.* **272** 211–21

[17] Fukunga K 1990 *Introduction to Statistical Pattern Recognition* (San Diego, CA: Academic)

[18] Gabbiani F, Metzner W, Wessel R and Koch C 1996 From stimulus encoding to feature extraction in weakly electric fish *Nature* **386** 564–7

[19] Gray C M and Singer W 1989 Stimulus-specific neuronal oscillations in orientation columns of cat visual cortex *Proc. Natl Acad. Sci. USA* **86** 1698–702
[20] Haag J and Borst A 1998 Active membrane properties and signal encoding in graded potential neurons *J. Neurosci.* **18** 7972–86
[21] Harris K D, Hirase H, Leinekugel X, Henze D A and Buzsáki G 2001 Temporal interaction between single spikes and complex spike bursts in hippocampal pyramidal cells *Neuron* **32** 141–9
[22] Hodgkin A L and Huxley A F 1952 A quantitative description of membrane current and its application to conduction and excitation in nerve *J. Physiol.* **117** 500–44
[23] Kamondi A, Acsády L, Wang X-J and Buzsáki Gy 1998 Theta oscillations in somata and dendrites of hippocampal pyramidal cells *in vivo*: activity-dependent phase-precession of action potentials *Hippocampus* **8** 244–60
[24] Kepecs A and Wang X-J 2000 Analysis of complex bursting in cortical pyramidal neuron models *Neurocomputing* **32** 181–7
[25] Kepecs A, Wang X J and Lisman J 2002 Bursting neurons signal input slope *J. Neurosci.* **22** 9053–62
[26] Kistler W, Gerstner W and van Hemmen J L 1997 Reduction of Hodgkin–Huxley equations to a threshold model *Neural Comput.* **9** 1069–100
[27] Larkum M E, Zhu J J and Sakmann B 1999 A new cellular mechanism for coupling input arriving at different cortical layers *Nature* **398** 338–41
[28] Lisman J E 1997 Bursts as units of neural information *Trends Neurosci.* **20** 38–41
[29] Livingstone M S, Freeman D C and Hubel D H 1996 Visual responses in V1 of freely viewing monkeys *Cold Spring Harbor Symp. Quant. Biol.* **61** 27–37
[30] Magee J C and Carruth M 1999 Dendritic voltage-gated ion channels regulate the action potential firing mode of hippocampal CA1 pyramidal neurons *J. Neurophysiol.* **82** 1895–901
[31] Mainen Z F and Sejnowski T F 1996 Influence of dendritic structure on firing pattern in model neocortical neurons *Nature* **382** 363–6
[32] Manwani A and Koch C 1999 Detecting and estimating signals in noisy cable structures II: Information theoretical analysis *Neural Comput.* **11** 1831–73
[33] Mel B W 1994 Information processing in dendritic trees *Neural Comput.* **6** 1031–85
[34] Metzner W, Koch C, Wessel R and Gabbiani F 1998 Feature extraction by burst-like spike patterns in multiple sensory maps *J. Neurosci.* **18** 2283–300
[35] Molden S, Fyhn M, Hollup S A, Moser M-B and Moser E I 2001 Place correlates of complex spikes in CA1 pyramidal cells *Soc. Neuro. Abstr.* **32** 643.4
[36] Otto T, Eichenbaum H, Wiener S I and Wible C G 1991 Learning-related patterns of CA1 spike trains parallel stimulation parameters optimal for inducing hippocampal long-term potentiation *Hippocampus* **1** 181–92
[37] Ovied H and Reyes A D 2002 Boosting of neuronal firing evoked with asynchronous and synchronous inputs to the dendrite *Nature Neurosci.* **5** 261–6
[38] Pinsky P F and Rinzel J 1994 Intrinsic and network rhythmogenesis in a reduced traub model for CA3 neurons *J. Comput. Neurosci.* **1** 39–60
[39] Reich D S, Mechler F, Purpura K P and Victor J D 2000 Interspike intervals, receptive fields, and information encoding in primary visual cortex *J. Neurosci.* **20** 1964
[40] Reich D S, Victor J and Kaplan E 1997 Response variability and timing precision of neuronal spike trains *in vivo J. Neurophys.* **77** 2836
[41] Reinagel P, Godwin D, Sherman S M and Koch C 1999 Encoding of visual information by LGN bursts *J. Neurophysiol.* **81** 2558–69
[42] Reinagel P and Reid R C 2000 Temporal coding of visual information in the thalamus *J. Neurosci.* **20** 5392
[43] Rinzel J 1987 *Morphogenesis and Neuroscience (Springer Mathematical Topics in Population Biology)* (Berlin: Springer)
[44] Schneidman E, Freedman B and Segev I 1998 Ion channel stochasticity may be critical in determining the reliability and precision of spike timing *Neural Comput.* **10** 1679–703
[45] Schwartz O, Chichilnisky E J and Simoncelli E 2002 Characterizing neural gain control using spike-triggered covariance *Advances in Neural Information Processing Systems* vol 14, ed T G Dietterich, S Becker and Z Ghahramani (Cambridge, MA: MIT Press)
[46] Shadlen M N and Newsome W T 1994 Noise, neural codes and cortical organization *Curr. Opin. Neurobiol.* **4** 569–79
[47] Sherman S M 2001 Tonic and burst firing: dual modes of thalamocortical relay *Trends Neurosci.* **24** 122–6
[48] Silva L R, Amitai Y and Connors B W 1991 Intrinsic oscillations of neocortex generated by layer 5 pyramidal neurons *Science* **251** 432–5

[49] Softky W 1994 Sub-millisecond coincidence detection in active dendritic trees *Neuroscience* **58** 13–41
[50] Stevens C and Zador A 1996 Information through a spiking neuron *Advances in Information Processing Systems* vol 8, ed Touretzky, Mozer and Hasselmo (Cambridge, MA: MIT Press)
[51] Traub R D, Wong R K S, Miles R and Michelson H 1991 A model of a CA3 hippocampal pyramidal neuron incorporating voltage-clamp data on intrinsic conductances *J. Neurophysiol.* **66** 635–50
[52] Troyer T W and Miller K D 1997 Physiological gain leads to high ISI variability in a simple model of a cortical regular spiking cell *Neural Comput.* **9** 971–83
[53] Turner R W, Maler L, Deerinck T, Levinson S R and Ellisman M H 1994 TTX-sensitive dendritic sodium channels underlie oscillatory discharge in a vertebrate sensory neuron *J. Neurosci.* **14** 6453–71
[54] Vaadia E and Abeles M 1987 Temporal firing patterns of single units, pairs and triplets of units in the auditory cortex *Isr. J. Med. Sci.* **23** 75–83